OPEN

Ternary Organic Solar Cells Based on a Wide-Bandgap Polymer with Enhanced Power Conversion Efficiencies

Hyeongjin Hwang, Dong Hun Sin, Chaneui Park & Kilwon Cho

A low-bandgap acceptor (ITIC) was added to a binary system composed of a wide-bandgap polymer (PBT-OTT) and an acceptor ($PC_{71}BM$) to increase the light harvesting efficiency of the associated organic solar cells (OSCs). A ternary blend OSC with an acceptor ratio of $PC_{71}BM$:ITIC = 8:2 was found to exhibit a power conversion efficiency of 8.18%, which is 18% higher than that of the binary OSC without ITIC. This improvement is mainly due to the enhanced light absorption and optimized film morphology that result from ITIC addition. Furthermore, an energy level cascade forms in the blend that ensures efficient charge transfer, and bimolecular and trap-assisted recombination is suppressed. Thus the use of ternary blend systems provides an effective strategy for the development of efficient single-junction OSCs.

Organic solar cells (OSCs) can be lightweight, flexible, transparent, and mass-producible[1–3]. Recent studies have reported single-junction OSCs with significantly increased power conversion efficiencies (PCEs) > 10%[4–8].

In a general approach to the fabrication of OSCs, the photoactive layer can be prepared by mixing a light-harvesting polymer as a donor and an electron-accepting fullerene derivative as an acceptor. However, such binary OSCs have relatively narrow light absorption windows, which restricts their photocurrent generation[9,10]. In order to increase their light absorption, tandem structures have been introduced. A bottom cell based on a wide-bandgap polymer and a top cell based on a narrow-bandgap polymer are linked in series, which results in complementary absorption of the solar spectrum and boosts the power conversion efficiency of the incorporated cells[11]. However, tandem structures have several drawbacks such as their complex fabrication process and high production costs, which limit their practical applications[12].

In the past few years, ternary blend OSCs have been developed that exhibit extended light absorption and do not require complicated fabrication processes[13–15]. The light absorption spectrum of the third component is generally complementary to that of the light-harvesting polymer and is introduced into the donor/acceptor binary blend[10]. The presence of the third component can result in the formation in combination with the other two components of an energy level cascade for charge transfer, and can also enhance the development of the film morphology. Furthermore, ternary single-junction OSCs can be fabricated with a process that is simpler than the complex processes required for the fabrication of tandem OSCs[16–18].

Recently, 3,9-bis(2-methylene-(3-(1,1-dicyanomethylene)-indanone))-5,5,11,11-tetrakis(4-hexylphenyl)-dithieno[2,3-d:2′,3′-d′]-s-indaceno[1,2-b:5,6-b′]dithiophene) (ITIC) was developed as a narrow-bandgap acceptor. ITIC exhibits strong light absorption in the infrared region and its energy level can be adjusted for compatibility with other absorbing materials, so ITIC-based OSCs have been found to exhibit outstanding performances[19–25]. However, ITIC exhibits high photovoltaic performance in combination with only very few polymers because its aggregation properties pose difficulties for the control of the film morphologies of ITIC-based blend films. Moreover, in some cases, ITIC-based OSCs exhibit relatively low fill factors (FFs) because of recombination losses and low electron mobilities[26].

For ITIC to act as an efficient acceptor, it is important to control its aggregation[27]. Such control can be achieved by mixing ITIC with [6,6]-phenyl-C_{71}-butyric acid methyl ester ($PC_{71}BM$), which has high miscibility with donor polymers. The resulting mixed acceptor can then act as a light harvester and be miscible with donor polymers without severe aggregation.

Department of Chemical Engineering, Pohang University of Science and Technology, Pohang, 37673, Korea. Hyeongjin Hwang, Dong Hun Sin and Chaneui Park contributed equally. Correspondence and requests for materials should be addressed to K.C. (email: kwcho@postech.ac.kr)
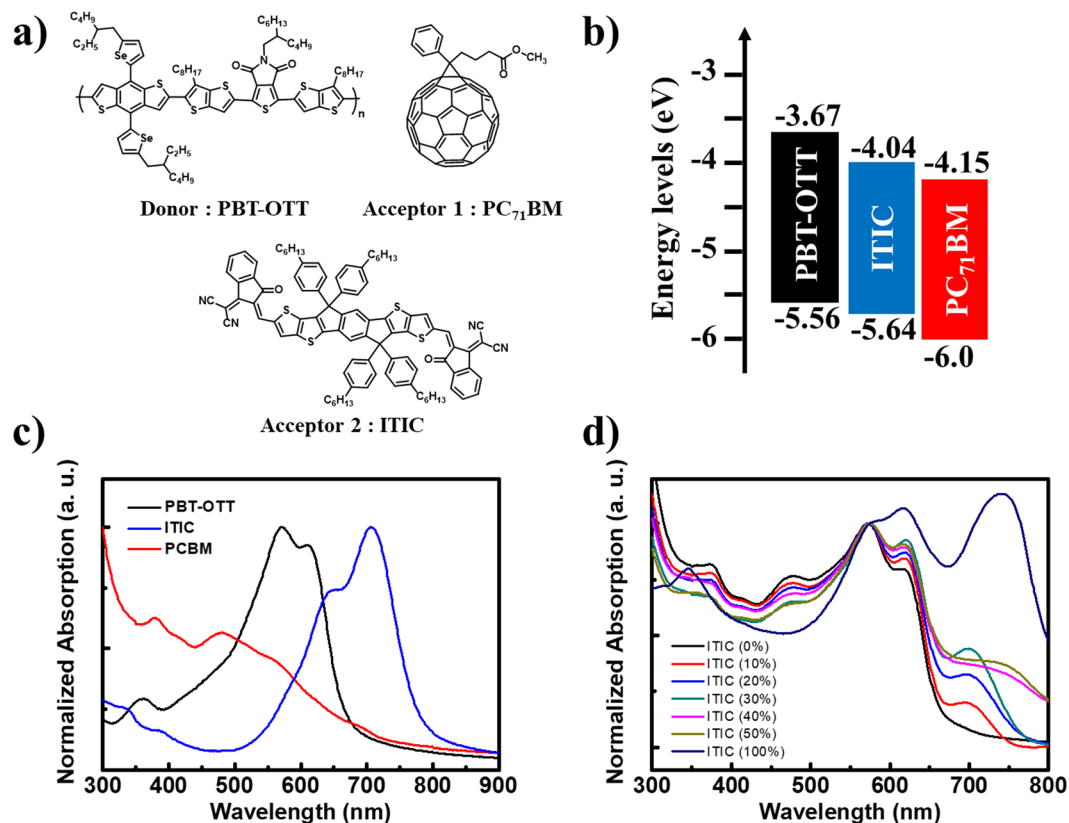
Figure 1. (**a**) Chemical structures of PBT-OTT, PC$_{71}$BM, and ITIC. (**b**) Energy levels diagrams for PBT-OTT, ITIC, PC$_{71}$BM. (**c**) UV-Vis absorption spectra of PBT-OTT, ITIC, and PC$_{71}$BM films. (**d**) UV-Vis absorption spectra of PBT-OTT:ITIC:PC$_{71}$BM with different ITIC contents (wt %); the number following "ITIC" in the legend represents the percentage of ITIC used in blend films.

In this study, we combined this mixed acceptor based on the narrow-bandgap ITIC and PC$_{71}$BM with a wide-bandgap polymer, PBT-OTT[28], and sought to optimize the light absorption and morphology of the resulting photoactive layer. The absorption of ITIC complements that of PBT-OTT ($300 \leq \lambda \leq 800$ nm) and forms an energy cascade that promotes charge transfer in the ternary blend. Here, we define [ITIC] as the ITIC content (wt/wt) relative to that of PC$_{71}$BM. [ITIC] was systematically varied from 0 to 100%. For [ITIC] = 20%, ITIC is well-mixed with PBT-OTT and PC$_{71}$BM, which results in an optimized film morphology and a ternary-blend-based OSC with a PCE of 8.18%, which is 18% higher than that of the binary-blend-based OSC. The charge generation, charge transport, and recombination dynamics of the OSC were characterized to determine the effects of the use of the ternary blend. These results demonstrate that the ternary blend approach is an effective strategy that enables the simple fabrication of highly efficient OSCs.

Results and Discussion

Optoelectric properties and the charge transfer mechanism. The chemical structures of PBT-OTT, PC$_{71}$BM, and ITIC are presented in Fig. 1a. The highest occupied molecular orbital (HOMO) energy levels of PBT-OTT and ITIC were determined from their onset oxidation potentials measured by cyclic voltammetry (CV), and their lowest unoccupied molecular orbital (LUMO) energy levels were determined from their optical bandgaps (Fig. 1b)[29]. The ternary blends provide broad and strong absorption covering the range of wavelengths from the visible to the near-infrared (Fig. 1c). The maximum absorptions of the PBT-OTT and ITIC films are at $\lambda = 512$ nm and 706 nm respectively. As the ITIC content of the PBT-OTT:PC$_{71}$BM blend increases, the intensity of absorption in the range $680 \leq \lambda \leq 760$ nm increases while that in the range $340 \leq \lambda \leq 510$ nm decreases and the intensity of the PBT-OTT shoulder peak adjacent to the maximum absorption peak in the film state strengthens.

The presence of the ITIC acceptor results in cascaded energy levels, in contrast to those of the PBT-OTT:PC$_{71}$BM blend (Fig. 1b). The LUMO energy level of ITIC is positioned between that of PBT-OTT and PC$_{71}$BM. Cascaded LUMO energy level alignment promotes electron transfer between the components of the bulk heterojunction blend and ensures efficient exciton splitting and charge transport to the electrodes[30]. The HOMO energy level of ITIC lies between that of PBT-OTT and PC$_{71}$BM, so holes are extracted efficiently from PC$_{71}$BM. To demonstrate that the energy levels of the three components are cascaded, we obtained the film photoluminescence (PL) spectra of PBT-OTT, ITIC, PC$_{71}$BM, PBT-OTT:ITIC (1:1), and PBT-OTT:PC$_{71}$BM (1:1) with excitation at 570 nm, which corresponds to the maximum absorption of PBT-OTT, and of ITIC:PC$_{71}$BM (1:1) with excitation at 705 nm, which corresponds to the maximum absorption of ITIC (Fig. 2). The emission of PBT-OTT is quenched without an increase in the ITIC PL signal and quenched completely without an increase
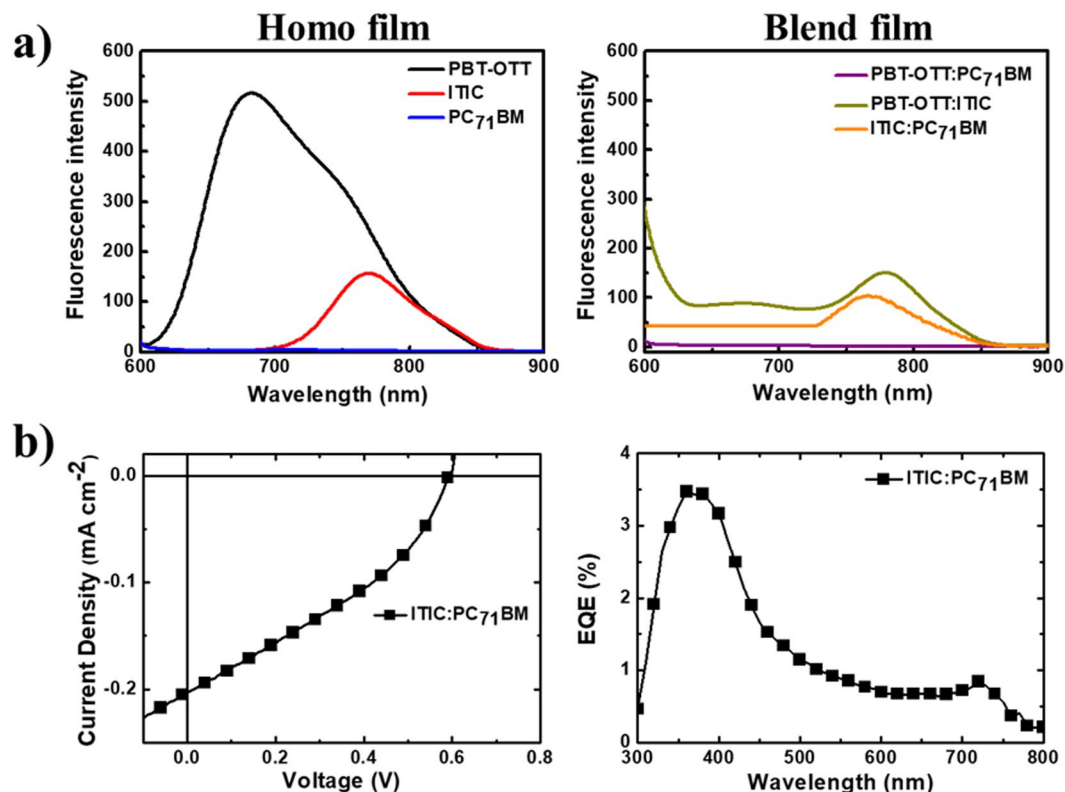
Figure 2. (**a**) Photoluminescence spectra of PBT-OTT, ITIC, $PC_{71}BM$, PBT-OTT:ITIC (1:1), PBT-OTT:$PC_{71}BM$ (1:1) excited at 570 nm, and ITIC:$PC_{71}BM$ (1:1) excited at 705 nm, and (**b**) photovoltaic properties of the ITIC:$PC_{71}BM$ binary device.

PBT-OTT:ITIC:$PC_{71}BM$	ITIC:$PC_{71}BM$ [wt%]	J_{SC} [mA cm^{-2}]	V_{OC} [V]	FF [%]	PCE$_{max}$ (PCE$_{avg}$)* [%]
1:0:1.5	0: 100	13.3 ± 0.3	0.83 ± 0.01	58.5 ± 3.2	6.74 (6.41 ± 0.43)
1:0.15:1.35	10: 90	13.9 ± 0.5	0.86 ± 0.01	63.6 ± 1.4	7.92 (7.59 ± 0.28)
1:0.3:1.2	20: 80	14.8 ± 0.2	0.87 ± 0.01	63.0 ± 1.2	8.18 (8.06 ± 0.14)
1:0.45:1.05	30: 70	14.5 ± 0.3	0.87 ± −0.1	55.5 ± 1.8	7.24 (7.02 ± 0.22)
1:0.6:0.9	40: 60	11.5 ± 0.7	0.88 ± 0.1	53.3 ± 2.0	5.60 (5.36 ± 0.24)
1:0.75:0.75	50: 50	8.28 ± 0.5	0.89 ± 0.1	42.1 ± 2.1	3.31 (3.08 ± 0.21)
1:1.5:0	100: 0	10.27 ± 0.4	0.97 ± 0.1	51.0 ± 2.1	5.43 (5.10 ± 0.36)

Table 1. Detailed photovoltaic parameters of PBT-OTT:ITIC:$PC_{71}BM$ based devices with different ITIC contents (wt%). *The values in parentheses stand for the average PCEs with standard deviations from over 12 devices.

in the $PC_{71}BM$ PL signal (Fig. 2a). These results confirm that photoinduced electrons can be transferred from PBT-OTT to ITIC and then to $PC_{71}BM$. OSC devices based on the ITIC:$PC_{71}BM$ blend were found to exhibit photodiode characteristics in their J-V curves and EQE peaks in the ranges $300 \leq \lambda \leq 450$ nm and $700 \leq \lambda \leq 800$ nm, which correspond to the absorption ranges of $PC_{71}BM$ and ITIC respectively. These results reveal that holes and electrons transfer from $PC_{71}BM$ to ITIC and from ITIC to $PC_{71}BM$ respectively. Further, considering that there is evidence for hole transfer from ITIC to PBT-OTT in the demonstration of a PCE of 5.43% for a device based on PBT-OTT:ITIC (Table 1) and also that the EQE increases in the range $700 \leq \lambda \leq 800$ nm (Fig. 3b) because ITIC exhibits high absorption in the PBT-OTT:ITIC blend (1:1) (Fig. 1c), we conclude that holes can transfer from $PC_{71}BM$ to ITIC and finally to PBT-OTT. Thus, an energy level cascade forms in the ternary blend system.

Photovoltaic properties. The photovoltaic efficiencies of ternary blend OSCs fabricated with the inverted structure ITO/ZnO/active layer (PBT-OTT:ITIC:$PC_{71}BM$)/MoOx/Al were evaluated. The overall donor-to-acceptor ratio in the active layer was fixed at 1:1.5 (wt/wt%). 3 vol % 1,8-diiodooctane (DIO) was used as a processing additive. In these ternary blends, the $PC_{71}BM$:ITIC ratio was varied: [ITIC] = 10, 20, 30, 40, 50, and 100 wt %. Figure 3a shows the current density (J) vs. voltage (V) characteristics of the OSCs with the different ITIC contents, and their photovoltaic parameters are summarized in Table 1. The binary reference device based
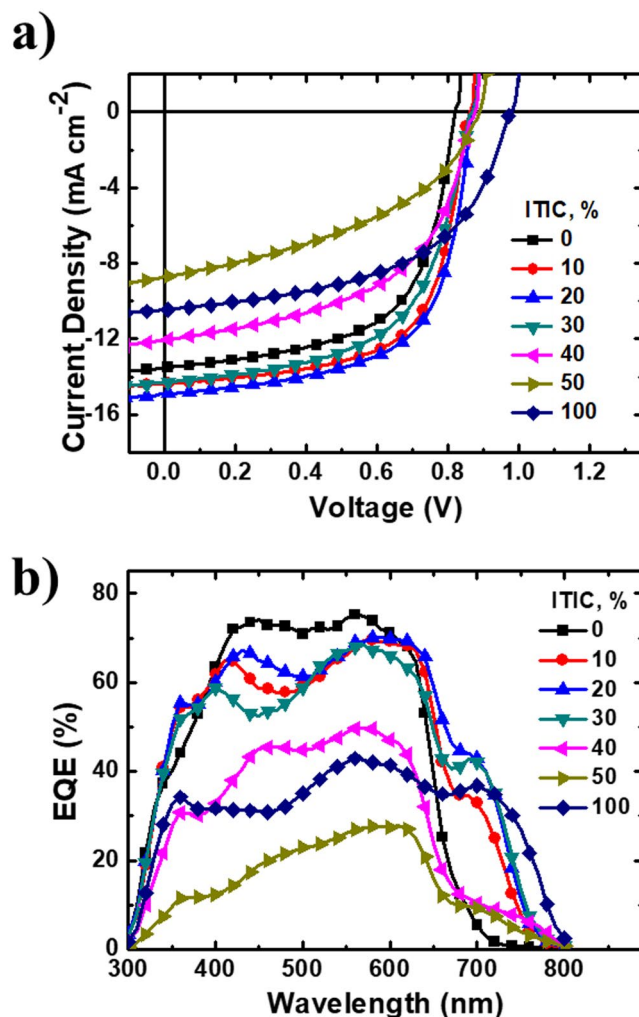
Figure 3. Photovoltaic performance of the ternary devices. (**a**) Characteristic J-V curves of the devices based on PBT-OTT:ITIC:PC$_{71}$BM with different ITIC weight ratio under illumination of AM 1.5 G, 100 mW/cm^2 light. (**b**) EQE curves of the ternary devices.

on PBT-OTT:PC$_{71}$BM was found to exhibit the following characteristics: PCE = 6.74% with J_{SC} = 13.53 mA cm^{-2}, V_{OC} = 0.82 V, and FF = 60.7%. For [ITIC] = 10%, the PCE increases to 7.92%, J_{SC} to 14.34 mA cm^{-2}, V_{OC} to 0.86 V, and FF to 64.49%. For [ITIC] = 20% the photovoltaic characteristics are optimal: PCE = 8.18%, J_{SC} = 14.93 mA cm^{-2}, V_{OC} = 0.87 V, and FF = 63.0%. These increases could be due to the expanded light absorption at wavelengths up to λ = 800 nm. For [ITIC] > 20%, the FF values decrease gradually; this trend is possibly due to a reduction of hole mobility measured by the space charge limited current (SCLC) method as [ITIC] increases (Fig. S1 and Table S2). For [ITIC] = 20%, the hole mobility μ_h is higher and μ_h/μ_e is close to 1 (Table S2). However, for [ITIC] = 50%, μ_h is reduced and μ_h/μ_e deviates from 1. We conclude that under the optimal conditions when [ITIC] = 20%, photo-generated charge carriers are extracted more efficiently to the electrodes in the device than at other [ITIC]. These phenomena are also affected by bimolecular recombination, which is discussed in Section 2.4. For [ITIC] > 20%, increases in the [ITIC] of the blend up to 50% simultaneously degrade the J_{SC} and FF values of the associated OSCs. V_{OC} gradually increases as [ITIC] increases, possibly because the high-lying LUMO of ITIC leads to charge transfer (CT) state with higher energy than that of PC$_{71}$BM at the donor polymer/acceptor molecule interface. In ternary blends, CT states can form at both PBT-OTT/ITIC and PBT-OTT/PCBM interface, and average CT energy determines final V_{OC}.

The overall EQEs for [ITIC] = 10, 20, and 30% in the ternary blend are significantly higher than those of the PBT-OTT:PC$_{71}$BM binary blend (Fig. 3b). This result demonstrates that more photogenerated excitons in the active layer dissociate to free charges and are collected by the electrodes, as indicated by the significant increase in EQE for the range $630 \leq \lambda \leq 800$ nm due to the increase in light absorption that results from the introduction of ITIC, and that the energy level cascade of PBT-OTT, ITIC, and PC$_{71}$BM improves the charge carrier transport.

Charge generation and dissociation dynamics. To investigate the improved J_{SC} of the ternary OSCs, the charge generation and dissociation of the OSCs with [ITIC] = 0, 20, 50, and 100% were assessed by determining the saturation current density J_{sat} and the charge dissociation probabilities $P(E, T)$. Figure 4a shows the photocurrent density (J_{ph}) versus effective voltage (V_{eff}) curves for these ternary devices. Here, J_{ph} is defined as $J_{ph} = J_L - J_D$,
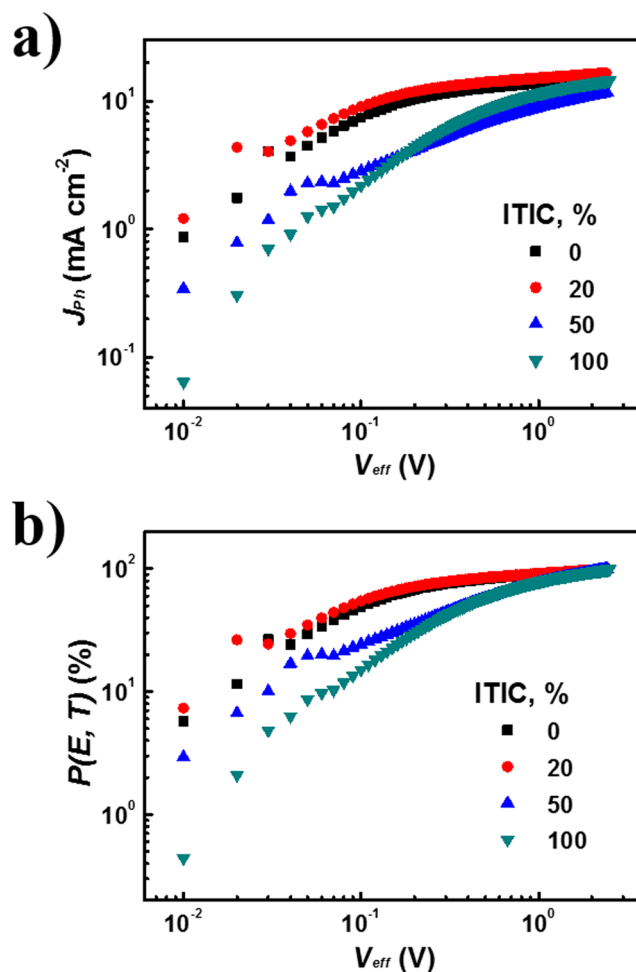
Figure 4. (**a**) Photocurrent density (J_{ph}) versus effective voltage (V_{eff}) characteristics. (**b**) $P(E, T)$ versus V_{eff}, where $P(E, T)$ determined by normalized J_{ph} with J_{sat} (J_{ph}/J_{sat}).

where J_L and J_D are the photocurrent densities under illumination and in the dark respectively. V_{eff} is defined as $V_{eff} = V_0 - V_a$, where V_0 is the voltage at which J_{ph} is zero and V_a is the applied bias voltage[31]. Generally, all photo-generated excitons are assumed to dissociate into free charge carriers at high V_{eff} (approximately 2 V), and then J_{sat} is only limited by the maximum exciton generation rate (G_{max}). As a result, J_{sat} equals to qLG_{max}, where q is the constant of the elementary charge and L is the active layer thickness[32]. G_{max} rises as [ITIC] rises to 20%: for [ITIC] = 0%, for $G_{max} = 9.51 \times 10^{27}$ m^{-3} s^{-1} and for $J_{sat} = 152.3$ Am^{-2}; for [ITIC] = 20%, for $G_{max} = 10.31 \times ^{27}$ m^{-3} s^{-1} and for $J_{sat} = 165.1$ Am^{-2}; for [ITIC] = 50%, for $G_{max} = 7.29 \times 10^{27}$ m^{-3} s^{-1} and for $J_{sat} = 116.8$ Am^{-2}; for [ITIC] = 100%, for $G_{max} = 9.08 \times 10^{27}$ m^{-3} s^{-1} and for $J_{sat} = 145.4$ A m^{-2}. The increase in G_{max} with [ITIC] suggests that the overall absorption and exciton generation increase in the ternary blend OSCs resulted from the complementary absorption that arose from the loading of a small amount of ITIC and the resulting energy cascade of PBT-OTT:ITIC:PC$_{71}$BM[33]. By normalizing J_{ph} with J_{sat}, $P(E, T)$ can be calculated (Fig. 4b)[33]. $P(E, T)$ is highest for [ITIC] = 20%; for [ITIC] = 0%, $P(E, T) = 88.7$; for [ITIC] = 20%, $P(E, T) = 90.5$; for [ITIC] = 50%, $P(E, T) = 74.7$; for [ITIC] = 100%, $P(E, T) = 79.5$. This trend indicates that the incorporation of low levels of ITIC increases the exciton dissociation at the donor/acceptor interfaces and ensures sufficient charge transport and collection at the electrodes in the active layer.

Charge recombination dynamics. To further investigate the effects of charge recombination dynamics on the efficiencies of the ternary OSCs, we obtained the J_{SC}-light illumination intensity plots for the four devices (Fig. 5a). It is known that J_{SC} has a power-law dependence on the light intensity (P_{light}), i.e. $J_{SC} \propto (P_{light})^S$, in OSCs[34]. In these devices, weak bimolecular recombination gives rise to $S \approx 1$. At low ITIC concentrations, ITIC has little effect on bimolecular recombination i.e., for [ITIC] = 0%, (the host binary blend, PBT-OTT:PC$_{71}$BM), $S = 0.98$ and at [ITIC] = 20%, $S = 0.99$, but for [ITIC] = 50%, $S = 0.90$ and for [ITIC] = 100%, $S = 0.91$; thus bimolecular recombination increases for ITIC concentrations above 20%. This trend is correlated with that for the films with aggregated morphologies, which is discussed in the following section. Increases in bimolecular recombination for [ITIC] > 20% are also related to the decreases in the J_{SC} and FF of the associated cells. Further, the bimolecular recombination trend is well correlated with those in μ_h and the ratio of μ_h to μ_e obtained using SCLC for the four devices.
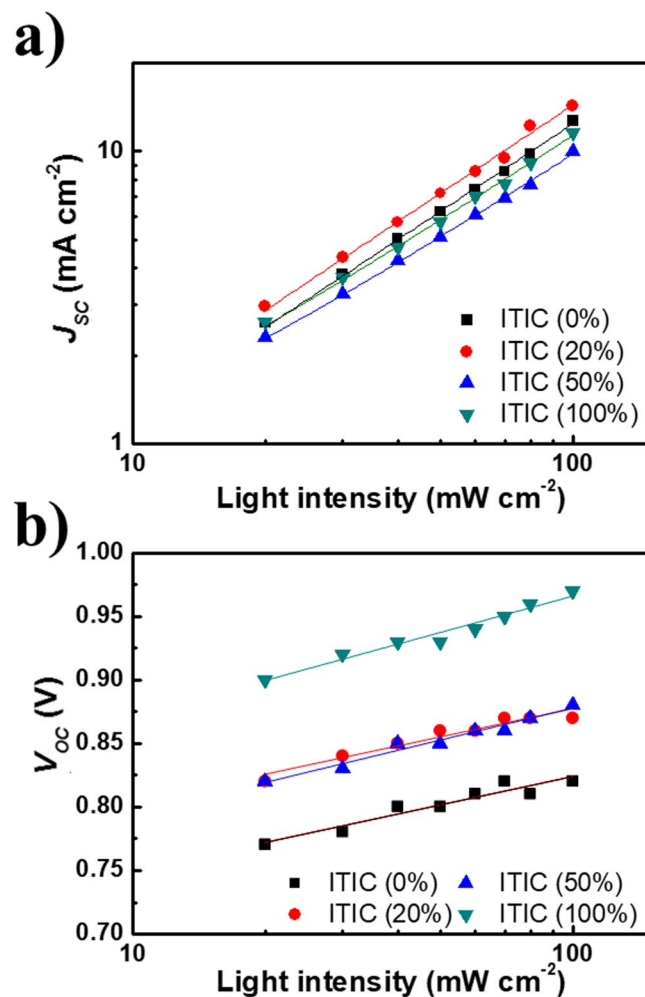
Figure 5. (**a**) Short-circuit current density (J_{sc}) versus light intensity and (**b**) open-circuit voltage (V_{oc}) versus light intensity for the ternary system.

The relationship between V_{OC} and P_{light} in OSCs with various [ITIC] is presented in Fig. 5b. The slope of each V_{OC} versus $\ln(P_{light})$ plot can be used to investigate the extent of trap-assisted recombination in the OSCs: a slope of $k_B T/q$ indicates whether trap-assisted recombination is dominant or not, where k_B is Boltzmann's constant, T is the absolute temperature. For Shockley-Read-Hall recombination or trap-assisted, the dependence of V_{OC} on P_{light} is stronger and results in the slope of $2k_B T/q$[34,35]. In our case, the blend with [ITIC] = 20% produces the smallest slope, 1.44 $k_B T/q$. These results show that the incorporation of a low concentration of ITIC in the host blend reduces the density of interfacial surface traps in the active layer; this reduction suppresses trap-assisted recombination and contributes to an increase in J_{SC}.

Thin film morphology and molecular ordering. To investigate how the presence of ITIC affects the film morphologies and photovoltaic properties of the blends, atomic force microscopy (AFM) was used. The PBT-OTT:PC$_{71}$BM films are homogeneous with a root-mean-square roughness (RMS) of 3.02 nm (Fig. 6a), which resulted from the high miscibility of PBT-OTT and PC$_{71}$BM[32]. For [ITIC] = 20%, the morphology is aggregated (RMS = 3.49 nm), which enables the development of an interpenetrating network and reduces the interfacial trap density in the active layer, and thereby improves the PCE of the associated OSCs. Increases in [ITIC] result in the formation of large aggregated regions and surfaces with high RMS values. These effects produce a significant reduction in FF (Section 2.2).

To further understand the results for the morphologies, optical microscopy (OM) was conducted for various weight ratios of ITIC and PC$_{71}$BM (Figs 6a and S2). For [ITIC] ≤ 20%, the resulting morphologies are almost clear, which indicates that the three components are well mixed. In contrast, obvious ITIC crystals form for [ITIC] > 30%; they are largest for [ITIC] = 40%, but decrease in size and increase in number for [ITIC] = 50% and 100%. For [ITIC] > 30%, the ITIC molecules do not mix well with PBT-OTT, so exciton dissociation is presumably inefficient and efficient electron transport pathways do not form.

To investigate the compatibility of PBT-OTT with ITIC and PC$_{71}$BM, the surface energies of PBT-OTT, ITIC, and PC$_{71}$BM were measured (Fig. S3; Table S5). Generally, the similar surface energies of components ensure good compatibility between the components. The obtained surface energies of PBT-OTT, ITIC, and PC$_{71}$BM were
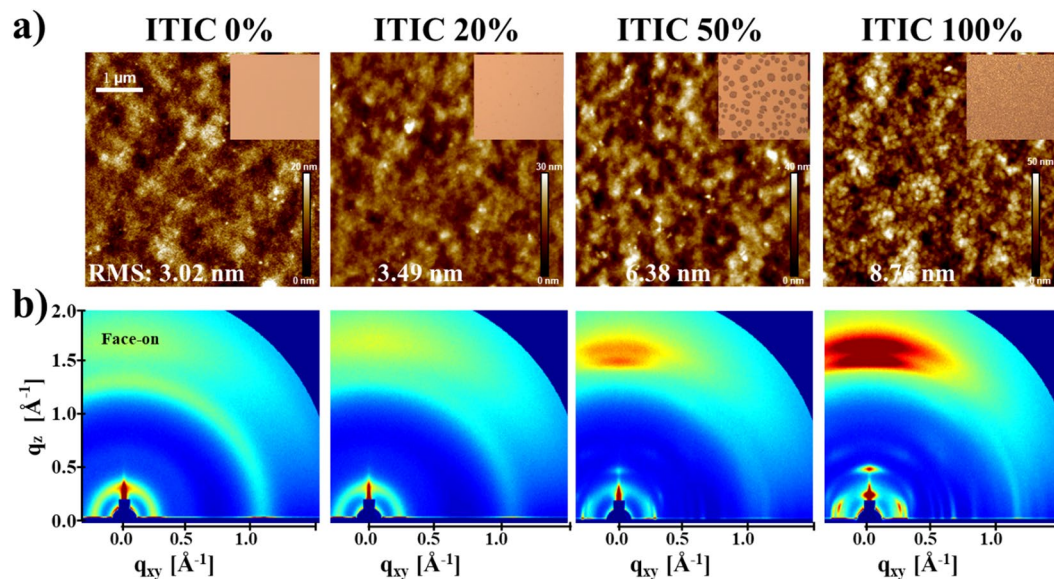
Figure 6. (**a**) AFM images and OM images (inset), and (**b**) GIWAXS data of PBT-OTT:ITIC:PC$_{71}$BM blend films with different ITIC contents (wt%).

36.4, 47.7, and 37.3 mN m^{-1}, respectively. The surface energy of PC$_{71}$BM is closer to that of PBT-OTT than that of ITIC, i.e., PBT-OTT is more miscible with PC$_{71}$BM than with ITIC. Hence, for [ITIC] > 30%, the phases separate and the film morphologies coarsen.

The crystal orientations and crystallite sizes of ternary blend films with various ITIC contents were studied by using grazing-incidence wide-angle X-ray scattering (GIWAXS) (Fig. 6b). The PBT-OTT:PC$_{71}$BM film exhibits a face-on orientation, which can increase the favorability of intra- and inter-molecular charge carrier transport by the polymers in OSC devices[32]. The addition of ITIC at a concentration of 20% increases the intensity of the scattering peaks attributed to the face-on orientation. This preferential face-on orientation enhances charge transport and thereby the photovoltaic properties, as demonstrated by the improved SCLC results (Fig. S1). Further increases in [ITIC] up to 100% result in gradual increases in the intensity of the peak due to the face-on orientation; this trend indicates that the face-on orientation of ITIC favors the face-on orientation of PBT-OTT, i.e. the presence of ITIC enhances the intensity of the peak due to the face-on orientation. Furthermore, for [ITIC] ≥ 50%, two separate peaks due to face-on PBT-OTT and ITIC in PBT-OTT:ITIC binary blend films are evident in the GIWAXS data (Figs S4 and 6b), which indicates that the miscibility of PBT-OTT and ITIC is reduced.

The sizes of the crystal domains of PBT-OTT and ITIC in the blend films were compared by using the Scherrer equation[36] to calculate the coherence lengths (CLs) (Table S6). Increases in [ITIC] from 40 to 100% result in gradually decreases in the CLs of ITIC. This trend is in agreement with the OM results in Fig. S4; for 0% ≤ [ITIC] ≤ 30%, the CLs of ITIC could not be calculated from the GI-WAX results, but the CLs of ITIC are expected to be small, as suggested by the OM results for 0% ≤ [ITIC] ≤ 30%. On the other hand, for 0% ≤ [ITIC] ≤ 20%, the CLs of PBT-OTT increase, but then decrease for 30% ≤ [ITIC]. As a result, the CLs of PBT-OTT mostly increase as the PC$_{71}$BM content in the blends is increased, which indicates that an improvement in the degree of the molecular ordering of PBT-OTT is obtained. This effect may explain the increase in the intensity of the shoulder on the PBT-OTT peak adjacent to the maximum absorption peak in the UV absorption spectra of the film states (Fig. 2d). Although their enhanced face-on orientation is facilitated by the addition of ITIC, addition of ITIC at concentrations greater than 30% reduces the PCE due to the reduced miscibility of PBT-OTT and ITIC.

Conclusion

We incorporated narrow-bandgap ITIC into the binary blend composed of wide-bandgap PBT-OTT and PC$_{71}$BM. It was found that the addition of ITIC extends the light absorption of the active layer and increases photocurrent generation; it also establishes an energy level cascade with PBT-OTT and PC$_{71}$BM, which promotes exciton dissociation and charge transfer. The optimum ITIC content (20%) results in a well-mixed and crystalline film morphology, which enhances the charge transport properties. Furthermore, the high-lying LUMO of ITIC, comparing with that of PC$_{71}$BM, boosts the V_{OC} of the ternary OSCs. The low electron mobility of ITIC is compensated by the high electron mobility of PC$_{71}$BM and balanced by the hole mobility of PBT-OTT. Therefore, charge recombination is effectively reduced and photo-generated charge carriers are efficiently collected at each electrode. The optimized ternary OSC with [ITIC] = 20% yields the highest PCE, 8.18%, which is 18% higher than that of the PBT-OTT:PC$_{71}$BM binary OSC. These results confirm the usefulness of the ternary blend approach to the development of OSCs.

Experimental Section

Materials. PBT-OTT was synthesized by the methods used in our previous work[28]. The number-average molecular weight ($\overline{Mn}$) of the synthesized polymer was 22,000 g mol^{-1}. All starting materials and reagents except for ITIC were purchased form Sigma-aldrich, Tokyo Chemical Industry Korea, Acros organics, and Frontier Scientific Inc., ITIC was purchased from Derthon Optoelectronic Materials Science Technology Co., LTD. All chemicals were used as received.

Device fabrication. ITO substrate was washed with detergent, distilled water, acetone, and isopropyl alcohol sequentially with ultra-sonication for 20 min at each step. After UV-O$_3$ treatment for 20 min, ZnO nanoparticles were deposited onto the ITO glass, evacuated for 4 hrs, and transferred into the N$_2$-filled glove-box. PBT-OTT:PC$_{71}$BM:ITIC blend solutions with controlled ratios were prepared in the chlorobenzene at 70 °C for overnight in the glove-box, and then deposited onto the ZnO-coated ITO glass. As a molecular additive, 1,8-diiodooctane (DIO) was added into the solution before depositing blend layer. The films were dried for 2 hrs. MoO$_3$ (3 nm) and Au (60 nm) were thermally evaporated through a patterned mask.

Characterization. All monomers synthesized in this work were characterized by ^{1}H NMR (600 MHz) and ^{13}C NMR (150 MHz) on a Bruker AVANCE III 600 spectrometer in chloroform-d solutions. The 1 H NMR chemical shift is shown in the d (ppm) unit relative to tetramethylsilane (TMS, d = 0) and refers to the peak signals corresponding to the non-deuterated remaining solvent. The polymers' absorption spectrum was obtained by an UV spectrophotometer (UV-3220, Mecasys). AFM images were obtained using a MultiMode 8 Scanning Probe Microscope (VEECO Instruments Inc.) by tapping mode.

Cyclic voltammetry analysis. The cyclic voltammetry (CV) data was obtained by using a PowerLab/AD instrument model system with the working electrode (glassy carbon disk), counter electrode (Pt wire), and reference electrode (Ag/Ag+) at a 50 mV s^{-1} potential scan speed in a solution of 0.1 M tetrabutylammonium hexafluorophosphate (n-Bu4NPF6)-anhydrous acetonitrile. Film was dropped from a 5.0 mg mL^{-1} warm CB solution onto the glassy carbon working electrode and dried before measurement under the nitrogen stream. With the use of the ferrocene/ferrocenium redox couple (Fc/Fc$^+$), the potential of the Ag/AgCl reference electrode was internally calibrated. The HOMO energy level was calculated by using the equation; HOMO $= -(4.80 + E_{onset})$.

References

1. Krebs, F. C., Espinosa, N., Hosel, M., Sondergaard, R. R. & Jorgensen, M. 25th Anniversary Article: Rise to Power - OPV-Based Solar Parks. *Adv. Mater.* **26**, 29–39 (2014).
2. Kippelen, B. & Bredas, J. L. Organic photovoltaics. *Energ. Environ. Sci.* **2**, 251–261 (2009).
3. Darling, S. B. & You, F. Q. The case for organic photovoltaics. *Rsc Adv* **3**, 17633–17648 (2013).
4. Lee, J. *et al.* Highly crystalline low-bandgap polymer nanowires towards high-performance thick-film organic solar cells exceeding 10% power conversion efficiency. *Energ. Environ. Sci.* **10**, 247–257 (2017).
5. Vohra, V. *et al.* Efficient inverted polymer solar cells employing favourable molecular orientation. *Nat. Photon* **9**, 403 (2015).
6. Zhao, J. B. *et al.* Efficient organic solar cells processed from hydrocarbon solvents. *Nat. Energy* **1**, 15027 (2016).
7. Jagadamma, L. K. *et al.* Polymer Solar Cells with Efficiency > 10% Enabled via a Facile Solution-Processed Al-Doped ZnO Electron Transporting Layer. *Adv. Energy Mater* **5**, 1500204 (2015).
8. Jin, Y. C. *et al.* Thick Film Polymer Solar Cells Based on Naphtho[1,2-c:5,6-c]bis[1,2,5]thiadiazole Conjugated Polymers with Efficiency over 11%. *Adv. Energy Mater* **7**, 1700944 (2017).
9. Hwang, H. *et al.* Fluorine-functionalization of an isoindoline-1,3-dione-based conjugated polymer for organic solar cells. *Org. Electron.* **59**, 247–252 (2018).
10. Ameri, T., Khoram, P., Min, J. & Brabec, C. J. Organic Ternary Solar Cells: A Review. *Adv. Mater.* **25**, 4245–4266 (2013).
11. Ko, S. J. *et al.* High-efficiency photovoltaic cells with wide optical band gap polymers based on fluorinated phenylene-alkoxybenzothiadiazole. *Energ. Environ. Sci.* **10**, 1443–1455 (2017).
12. Yang, J. *et al.* A Robust Inter-Connecting Layer for Achieving High Performance Tandem Polymer Solar Cells. *Adv. Mater.* **23**, 3465 (2011).
13. Kim, M. *et al.* Nonfullerene/Fullerene Acceptor Blend with a Tunable Energy State for High-Performance Ternary Organic Solar Cells. *Acs Appl. Mater. Interfaces* **10**, 25570–25579 (2018).
14. Lee, H., Park, C., Sin, D. H., Park, J. H. & Cho, K. Recent Advances in Morphology Optimization for Organic Photovoltaics. *Adv. Mater.* **30**, 1800453 (2018).
15. Yang, L. Q., Yan, L. & You, W. Organic Solar Cells beyond One Pair of Donor-Acceptor: Ternary Blends and More. *J. Phys. Chem. Lett.* **4**, 1802–1810 (2013).
16. Liu, S. H. *et al.* Enhanced efficiency of polymer solar cells by adding a high-mobility conjugated polymer. *Energ. Environ. Sci.* **8**, 1463–1470 (2015).
17. Lu, L. Y., Chen, W., Xu, T. & Yu, L. P. High-performance ternary blend polymer solar cells involving both energy transfer and hole relay processes. *Nat. Commun.* **6**, 7327 (2015).
18. Mai, J. Q. *et al.* High efficiency ternary organic solar cell with morphology-compatible polymers. *J. Mater. Chem. A* **5**, 11739–11745 (2017).
19. Hou, J. H., Inganas, O., Friend, R. H. & Gao, F. Organic solar cells based on non-fullerene acceptors. *Nat. Mater.* **17**, 119–128 (2018).
20. Gao, L. *et al.* High-Efficiency Nonfullerene Polymer Solar Cells with Medium Bandgap Polymer Donor and Narrow Bandgap Organic Semiconductor Acceptor. *Adv. Mater.* **28**, 8288–8295 (2016).
21. Liu, T. *et al.* Ternary Organic Solar Cells Based on Two Compatible Nonfullerene Acceptors with Power Conversion Efficiency > 10%. *Adv. Mater.* **28**, 10008–10015 (2016).
22. Zhao, F. W. *et al.* Single-Junction Binary-Blend Nonfullerene Polymer Solar Cells with 12.1% Efficiency. *Adv. Mater.* **29**, 1700144 (2017).
23. Yao, H. F. *et al.* Achieving Highly Efficient Nonfullerene Organic Solar Cells with Improved Intermolecular Interaction and Open-Circuit Voltage. *Adv. Mater.* **29**, 1700254 (2017).
24. Xu, X. P. *et al.* Realizing Over 13% Efficiency in Green-Solvent-Processed Nonfullerene Organic Solar Cells Enabled by 1,3,4-Thiadiazole-Based Wide-Bandgap Copolymers. *Adv. Mater.* **30**, 1703973 (2018).
25. Jang, B. *et al.* A High Dielectric N-Type Small Molecular Acceptor Containing Oligoethyleneglycol Side-Chains for Organic Solar Cells. *Chin. J. Chem* **36**, 199–205 (2018).

26. Lu, H. *et al*. Ternary-Blend Polymer Solar Cells Combining Fullerene and Nonfullerene Acceptors to Synergistically Boost the Photovoltaic Performance. *Adv. Mater.* **28**, 9559 (2016).
27. Cnops, K. *et al*. 8.4% efficient fullerene-free organic solar cells exploiting long-range exciton energy transfer. *Nat. Commun.* **5**, 3406 (2014).
28. Hwang, H. *et al*. Synergistic effects of an alkylthieno[3,2-b]thiophene pi-bridging backbone extension on the photovoltaic performances of donor-acceptor copolymers. *J. Mater. Chem. A* **5**, 10269–10279 (2017).
29. Kim, H. G. *et al*. Energy Level Engineering of Donor Polymers via Inductive and Resonance Effects for Polymer Solar Cells: Effects of Cyano and Alkoxy Substituents. *Chem. Mater.* **27**, 6858–6868 (2015).
30. Ahir, S. V., Tajbakhsh, A. R. & Terentjev, E. M. Self-assembled shape-memory fibers of triblock liquid-crystal polymers. *Adv. Funct. Mater.* **16**, 556–560 (2006).
31. Lu, L. Y., Luo, Z. Q., Xu, T. & Yu, L. P. Cooperative Plasmonic Effect of Ag and Au Nanoparticles on Enhancing Performance of Polymer Solar Cells. *Nano Lett.* **13**, 59–64 (2013).
32. Wu, J. L. *et al*. Surface Plasmonic Effects of Metallic Nanoparticles on the Performance of Polymer Bulk Heterojunction Solar Cells. *Acs Nano* **5**, 959–967 (2011).
33. Shrotriya, V., Yao, Y., Li, G. & Yang, Y. Effect of self-organization in polymer/fullerene bulk heterojunctions on solar cell performance. *Appl. Phys. Lett.* **89**, 063505 (2006).
34. Riedel, I. *et al*. Effect of temperature and illumination on the electrical characteristics of polymer-fullerene bulk-heterojunction solar cells. *Adv. Funct. Mater.* **14**, 38–44 (2004).
35. Koster, L. J. A., Mihailetchi, V. D., Ramaker, R. & Blom, P. W. M. Light intensity dependence of open-circuit voltage of polymer: fullerene solar cells. *Appl. Phys. Lett.* **86**, 123509 (2005).
36. Nagiri, R. C. R., Yambem, S. D., Lin, Q. Q., Burn, P. L. & Meredith, P. Room-temperature tilted-target sputtering deposition of highly transparent and low sheet resistance Al doped ZnO electrodes. *J. Mater. Chem. C* **3**, 5322–5331 (2015).

Acknowledgements

Author Contributions

H. Hwang, D.H. Sin, and C. Park contributed equally to this work, which was supervised by K. Cho. H. Hwang synthesized the donor polymer used in this study. D.H. Sin and C. Park fabricated and characterized associated photovoltaic devices. All authors contributed writing and reviewing the manuscript.

Additional Information

Supplementary information accompanies this paper at https://doi.org/10.1038/s41598-019-48306-x.

Competing Interests: The authors declare no competing interests.

Publisher's note: Springer Nature remains neutral with regard to jurisdictional claims in published maps and institutional affiliations.